Building and Environment 206 (2021) 108320

Contents lists available at ScienceDirect

Building and Environment

journal homepage: www.elsevier.com/locate/buildenv

3D characterization of a Boston Ivy double-skin green building facade using a LiDAR system

Gabriel Pérez [a], Alexandre Escolà [b], Joan R. Rosell-Polo [b], Julià Coma [a], Roger Arasanz [c], Bernat Marrero [c], Luisa F. Cabeza [d], Eduard Gregorio [b,*]

[a] Department of Computer Science and Industrial Engineering, University of Lleida, C/Jaume II 69, 25001, Lleida, Catalonia, Spain
[b] Research Group in AgroICT & Precision Agriculture, Department of Agricultural and Forest Engineering, University of Lleida – Agrotecnio-CERCA Center, 25198, Lleida, Catalonia, Spain
[c] Polytechnic School at the University of Lleida, C/Jaume II 69, 25001, Lleida, Catalonia, Spain
[d] GREiA Research Group, University of Lleida, C/Pere de Cabrera s/n, 25001, Lleida, Catalonia, Spain

ARTICLE INFO

Keywords:
Canopy 3D-modelling
LiDAR
Vertical greening systems (VGS)
Green facades
Buildings

ABSTRACT

On the way to more sustainable and resilient urban environments, the incorporation of urban green infrastructure (UGI) systems, such as green roofs and vertical greening systems, must be encouraged. Unfortunately, given their variable nature, these nature-based systems are difficult to geometrically characterize, and therefore there is a lack of 3D objects that adequately reflect their geometry and analytical properties to be used in design processes based on Building Information Modelling (BIM) technologies. This fact can be a disadvantage, during the building's design phase, of UGIs over traditional grey solutions. Areas of knowledge such as precision agriculture, have developed technologies and methodologies that characterize the geometry of vegetation using point cloud capture. The main aim of this research was to create the 3D characterization of an experimental double-skin green facade, using LiDAR technologies.

From the results it could be confirmed that the methodology used was precise and robust, enabling the 3D reconstruction of the green facade's outer envelope. Detailed results were that foliage volume differences in height were linked to plant growth, whereas differences in the horizontal distribution of greenery were related to the influence of the local microclimate and specific plant diseases on the south orientation. From this research, along with complementary previous research, it could be concluded that, generally speaking, with vegetation volumes of 0.2 m^3/m^2, using Boston Ivy (*Parthenocissus Tricuspidata*) under Mediterranean climate, reductions in external building surface temperatures of around 13 °C can be obtained and used as analytic parameter in a future 3D-BIM-object.

1. Introduction

In just over a decade there are likely to be around 8.5 billion people on earth, and 9.8 billion in 2050, compared to 7.8 billion today [1]. Given that by 2050, up to 6.7 billion people are expected to be living in cities (against a rural population of 3.1 billion) [2], Sustainable Development Goal 11 calls for making cities and human settlements inclusive, safe, resilient and sustainable [3].

Urban green infrastructure (UGI) is a set of elements that contribute to improving the environment in cities through the provision of multiple ecosystem services to the urban space, by reducing the urban heat island (UHI) effect, capturing pollutants and reducing CO_2 emissions, improving the control of urban rainwater runoff, decreasing traffic noise, and supporting biodiversity, among other benefits [4–7].

In recent decades, the possibility of integrating greenery into building skins, by means of green roofs and vertical greening systems (green walls and green facades), has become an innovative way to contribute to a more efficient use of urban space in cities. On a building level, greenery also provides multiple advantages, such as thermal and acoustic insulation, the protection of building skin materials, aesthetic effects and an increase in the property's value [4,8,9].

Among this set of new integrated building vegetation systems, double-skin green facades stand out for being easy to implement and maintain as well as for their high shading capacity, passively

* Corresponding author.
E-mail address: eduard.gregorio@udl.cat (E. Gregorio).

https://doi.org/10.1016/j.buildenv.2021.108320
Received 21 May 2021; Received in revised form 26 August 2021; Accepted 31 August 2021
Available online 2 September 2021
0360-1323/© 2021 The Authors. Published by Elsevier Ltd. This is an open access article under the CC BY license (http://creativecommons.org/licenses/by/4.0/).

contributing to large energy savings in buildings [10–13]. From previous studies on the main parameters that influence the thermal performance of this typology of green facades, it was concluded that plant foliage density, characterized by means of the Leaf Area Index (LAI), could be used as the main parameter describing the performance of these systems [10,14].

On the other side, in recent years, in parallel with the development of a more sustainable architecture and construction, 3D design has been consolidated as one of the strategies to incorporate the concept of "designing processes" rather than objects, considering already in the design phase the entire life cycle of buildings and their environmental impacts [15–17].

Thus, the processes of architectural design and urban planning are increasingly based on the use of Building Information Modelling (BIM) technologies which not only make it possible to design in three dimensions, but also to simulate the future behaviour, namely thermal, acoustic, etc., of buildings or cities during the design phase. Regarding this fact, some previous authors have highlighted the importance, and the need, to model vegetation at different scales (urban, district, street and building) in order to be able to make subsequent simulations based on BIM models on the effect of greenery on both the urban heat island effect reduction and the building energy-saving [18].

It has been widely acknowledged that BIM technologies are revolutionizing the landscape of building design and information management in the global architecture, engineering, and construction (AEC) industry [19,20]. Nevertheless, there still a knowledge gap regarding how to move from real objects to virtual objects in order to be able to properly model the construction systems, and to consequently shift BIM technologies from being a simple utopia to a reality in the building sector [21].

For this reason, some authors have stressed the importance of properly designing and developing BIM objects, so that they can be used efficiently in smart design processes, avoiding extremely heterogeneity between objects, in terms of geometry and information provided, and that can be easily included in the most used and open access BIM-object libraries [19,20]. Wang et al. [20] pointed out how a BIM object should be designed and developed in order to be useful and easily included in BIM object libraries. They identified three BIM object parameters that are critical to defining a BIM object, namely the identification, geometry and representation, and the behaviour.

In this context, in which architectural and building design decisions mainly depend on the available information in the early phases of the project, not only about the geometry of the architectural elements (dimensions and shape), but also on their properties (thermal, acoustic, etc.), these construction systems based in nature, such as green facades, are at a clear disadvantage in any choice of the designer over the traditional systems of grey infrastructure, e.g. shadow slats (Fig. 1) [22]. Thus, the complexity underlying greenery growth and natural processes, usually characterized by a lack of suitable information on technologies, processes, benefits, negative impacts, costs, maintenance, etc. [23], often leads to a bias in the designer's decisions toward grey infrastructure solutions, which offer more reliable expectancies from the point of view of their future performance.

In addition to this lack of trust towards nature-based solutions during the building design phase, it is also remarkable the difference between the current available quantity of grey infrastructure 3D BIM-objects in reference to the few relating to green infrastructure (Fig. 1) [22]. Whereas thousands of companies have faced the development of 3D objects during the last years, only few related to greenery construction systems can be found. In addition, in the most common databases of BIM objects, only a few referring to UGI elements can be found (bimobject [24], NBS National BIM Library [25], among others).

Moreover, the quality of these BIM-objects, both in terms of geometric design and the included information, is also higher for the grey systems.

Therefore, designers have during the design phase an easy access to a large palette of 3D-objects relating to grey infrastructure construction systems, whereas they are currently unavailable in the case of green infrastructure.

As a result, there is a real need for research on the development of reliable 3D-objects relating to urban green infrastructure systems, both on drawing designs and on information included. The opportunity to incorporate parametric information about the ecosystem services provided by these systems will make it possible to include these systems during the urban and building design phase, conducting simulations of their performance. As an example, in Fig. 2 a green facade 3D-object is showed. In this case and due to the difficulty to characterize geometrically the volume of the vegetation, the green facade volume was simplified in two parallel irregular volumes of different height and of variable thickness, which can be manually adapted by the user (Fig. 2 - right). Unfortunately, in this case there is no parameter that allows to correlate this simplified volume with the benefits provided by the green element (thermal, acoustic, etc.).

Thus, and looking for the design of a future BIM 3D-object, the possibility of obtaining an actual 3D model ("modelling") of the green facade to later include analytic properties ("information"), such as the LAI parameter, and to link this parameter to the energy savings provided [10–13], and/or the acoustic insulation performance [26], among other benefits, stands out as a realistic possibility that is worth being researched.

This study addresses the first phase and one of the most important in the development of a BIM object, which is the geometric characterization of the building element, in this case an existing double-skin green facade.

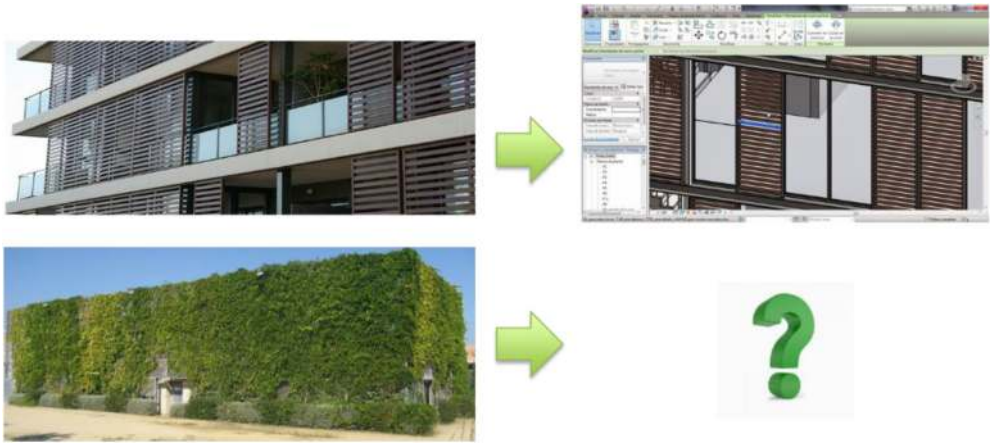


Fig. 1. Lack of 3D-objects for green infrastructure [22].

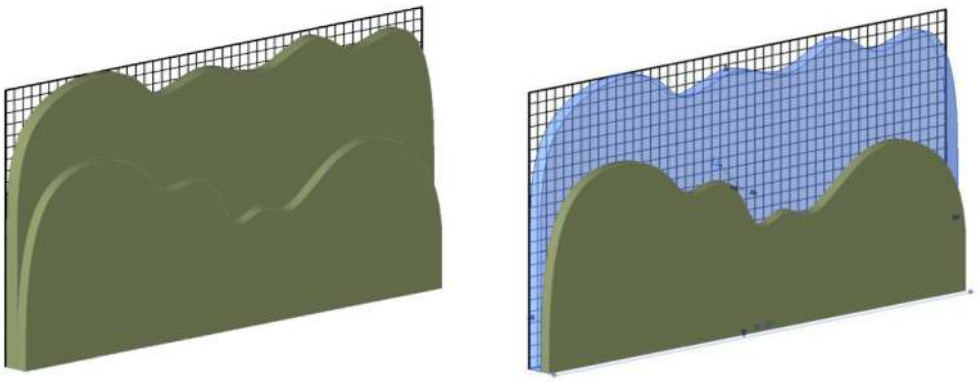


Fig. 2. Example of green facade 3D-object.

Previous studies have highlighted the use of point cloud capture methods to characterize complex architectural shapes that can be later used to create BIM objects [27]. However, for this purpose and considering the possibility of precisely characterizing the complex three-dimensional structure of vegetation, also in the field of precision agriculture, useful methodologies are used to obtain accurate models of the plants' foliage [28]. The information obtained from these 3D models is of great interest in making decisions regarding crop management [29,30], being able to be used to apply smart agricultural techniques, such as the precise application of plant protection products [31], to conduct simulations of plant growth [32] and final yield assessments [33], among other applications. In previous studies, different 3D sensors were used to perform this three-dimensional characterization, such as Light Detection and Ranging (LiDAR) systems, from which point clouds were obtained, which, once processed, enable the three-dimensional representation of the scanned vegetation to be analysed [34].

The operating principle of LiDAR systems is similar to Radio Detection and Ranging (RADAR), but they use laser light instead of radio waves. From the speed of light or the phase shift of backscattered light, LiDAR systems estimate the distance between the sensor and the detected object by measuring the time it takes for the light emitted by the sensor to reach the object and return to the sensor [30]. Therefore, they have a source that emits a laser light beam and a photodetector to detect returns and their intensity. In most LiDAR systems, the laser beam is emitted sequentially in several directions within a plane, usually by means of a rotating mirror, achieving the measurement of the distances of objects located in the plane in which the scan is performed; this is why they are frequently called laser scanners or LiDAR scanners.

3D characterization systems based on LiDAR scanners can be classified according to the type of platform on which they are boarded. Thus, we speak about Airborne Laser Scanners (ALS) and Spaceborne Laser Scanners (SLS) in the case that LiDAR scanners perform measurements from an approximately zenithal position from a height of the order of a few meters to several kilometers, boarded on an aircraft (drone, helicopter, plane) or on a satellite, respectively. Alternatively, Terrestrial Laser Scanners (TLS) perform measurements from the ground, either stationary or mobile, on board of a terrestrial vehicle (in this case, we speak about Mobile Terrestrial Laser Scanners, MTLS) [35] or even carried by humans (Portable Terrestrial Laser Scanners, PTLS). ALS have the advantage that they allow 3D measurements of large areas in a short time, although their spatial resolution, accuracy and precision is usually limited for certain applications. ALS have been used for decades in architecture [36,37], civil engineering [38], archaeological heritage [39], geosciences [40] and forestry [41,42], among others. On the other hand, TLS perform measurements in smaller areas (usually ranging from a few square meters to a few hundred square meters) but with a much larger spatial resolution than ALS. TLS has been used for decades in a multitude of fields, being architecture [43–47], civil engineering [48,49], forestry [50,51] and, more recently, agriculture [52–54] some of the most active fields, along with metrology, robotics and autonomous vehicles. Although both ALS and TLS systems obtain the external 3D characteristics of the measured targets, in certain applications (such as in the case of architecture and civil engineering), TLS even allow measurements to be made to characterize the interior of buildings.

Many LiDAR sensors are 2D. This means that they scan objects in a plane. To obtain 3D models of the objects it is necessary to move the sensor constituting MTLS or PTLS, so that, by joining the measurements of the different scanned planes, a 3D model of the object is obtained [52–54]. There are also LiDAR sensors that perform the measurements directly in 3D, from which an MTLS can also be constituted. Many 3D TLS perform the measurements in a stationary position which is changed around the measured object in order to complete its 3D model. These 3D TLS allow obtaining 3D models with a higher accuracy than MTLS or PTLS [35]. However, the acquisition time of stationary TLS is higher than MTLS or PTLS. The results of the measurements obtained with an MTLS consist of a set of points, called a "point cloud", each corresponding to a measurement of a specific point on the surface of the object, thus providing the 3D model of the measured object. In MTLS, LiDAR scanners usually work synchronously with an Inertial Measurement Unit (IMU) and a Global Positioning System (GNSS). The former allows tilting errors to be corrected and the latter allows spatial coordinates to be assigned to each point in the cloud to facilitate further analysis and use.

The measurement of plant characteristics with LiDAR scanners makes it possible to obtain their three-dimensional models and extract relevant parameters, both geometric (i.e. width, height, depth, volume) and structural (i.e. structure and geometry of plants, leaf density, penetration capacity of light) [35,55].

Since this methodology makes it possible to obtain 3D models of vegetation (leaf density) using a cloud of points, it was thought opportune and innovative to apply it in the field of sustainable construction and urban green infrastructures, to obtain the three-dimensional characterization of a double-skin green facade.

Therefore, the main objective of this research was to geometrically characterize a double-skin green facade using an MTLS typically applied in precision agriculture, in order to obtain a reliable three-dimensional representation of the foliage.

2. Materials and methods

2.1. Double-skin green facade description

There are different strategies for applying vegetation vertically on a building. As a basic first division, two main groupings can be established between green walls (living walls) and green facades, the former systems requiring more intensive levels of maintenance than the latter, which are more extensive [10]. Green walls are usually designed to support shrubs, so they are usually made up of plastic prefabricated modules

filled with substrate or covered in geotextile felts, in order to retain water and provide physical support to this plant typology (Fig. 3). On the other hand, climber species are mainly used for green facades. On the so-called *traditional green facade,* the building facade material is directly used as support, while on a *double-skin green facade,* a lightweight support structure allows plants to develop at a certain distance from the building wall.

Double-skin facades basically imply the contemporary adaptation of traditional systems, being very promising due to their simple designs, low investment, minimum extensive maintenance, and low interaction with architectural elements [56,57].

For the experiment presented in this paper, a double-skin green facade was used [58]. To provide support to the plants, a lightweight steel mesh was anchored using screws at 25 cm from the building wall, creating an intermediate space between the green screen and the building facade wall (Fig. 4).

The double-skin green facade covered the east, south and west sides of a fully monitored experimental cubicle, previously used to study the thermal performance of this system [10], the selected species being Boston ivy (*Parthenocissus Tricuspidata*), a deciduous species well-adapted to the continental Mediterranean climate. Plants reached their maximum development during summer 2015 (Fig. 5), and since then every year the three cubicle orientations became completely covered from April to November.

2.2. Sensoring system

The measurement system consisted of a self-developed MTLS composed of a LiDAR scanner and a real-time kinematics global navigation satellite system (RTK-GNSS), along with a personal computer, mounted on a self-propelled hybrid vehicle whose speed could be adjusted by the user over a wide range (Fig. 6).

The LiDAR scanner used is a UTM30-LX-EW (HOKUYO, Osaka, Japan). This sensor has a range of 30 m and performs 40 scans per second (40 Hz) in an almost vertical plane perpendicular to the direction of movement. Its field of view is 270° with an angular resolution of 0.25°, which enables 1081 distance measurements per scan (giving an acquisition rate of 43,240 points s^{-1}), each expressed in polar coordinates, i.e., the sensor determines the angle and distance of each measured point with respect to the sensor. The RTK-GNSS system used is a GNSS 1200+ (Leica Geosystems AG, Heerbrugg, Switzerland), which provides absolute coordinates and UTC time (synchronized with LiDAR) with a frequency of 20 Hz and an accuracy of approx. 20 mm.

The UTM30-LX-EW was mounted on a vertical mast firmly attached to the mobile platform, at a height of 170 cm above the ground and 31.5 cm below the receiving antenna of the RTK-GNSS rover. Table 1 summarizes the main characteristics of the developed MTLS system.

Two field trials were conducted. The first one was carried out in winter (December), with the facade without vegetation (Fig. 5b). In this trial, the UTM coordinates of the upper corners of the facades and the steel mesh were recorded. The second trial was conducted in the late summer period (September), when the greenery was completely developed (Fig. 5a). Both trials were performed by moving the MTLS along a rectilinear trajectory parallel to each of the facades, at an approximate distance of 4.5 m. Each scan provided measurements on a vertical plane perpendicular to the direction of advancement, that is, perpendicular to the green facades. The speed of the MTLS was 0.15 m/s, resulting in a distance between two consecutive scans of approximately 3.8 mm. The measurements were replicated to assess the repeatability of the system. Thus, two replicates of each facade were performed (rep 1 and rep 2).

2.3. Data processing

2.3.1. Generation of point clouds

The absolute coordinates determined by the receiver at the GNSS antenna were transferred to the LiDAR sensor and, from there, to the detected points of the point cloud. Both UTM30-LX-EW and GNSS1200+ were connected to a laptop with a software developed specifically to control and acquire data from the sensors, written in LabVIEW (National Instruments, Austin, USA), which combines and stores the coordinates of the RTK-GNSS receiver and LiDAR data. Therefore, each of the measured points was georeferenced in absolute rectangular coordinates with an approximate accuracy of ±50 mm (from Table 1: ±30 mm for the accuracy of the sensor and ±20 mm for the RTK-GNSS receiver). The scan of each facade generated a single file of about six million points. By fusing the points of the four facade orientations, as well as those describing the ground layer, a 3D image of the whole green facade was obtained.

2.3.2. Computing the vegetative volume

This section describes the steps followed to process the point clouds with the aim of characterizing the vegetative volume of the double-skin green facade:

1. The cubicle walls were 3D modelled by means of 3 m × 3 m planes. The walls were initially positioned departing from the GNSS coordinates of their upper vertices. Fine positioning of the walls was



Fig. 3. Examples of vertical greenery systems on a building: a) green wall, b) traditional skin-facade, and c) double-skin facade.



Fig. 4. Double-skin facade under study. Construction system detail and general view during growth phase.



Fig. 5. Double-skin green facade under study, completely developed from summer 2015. (a) East facade in summer. (b) East facade in winter. (c) North view and side view of east facade in summer. (d) Middle space, free of leaves, between the building facade wall and the steel mesh, in summer.

achieved by using the georeferenced point clouds of the facade without vegetation.

2. Then, the measurements of the facade with completely developed vegetation were processed. The point clouds of the three vegetated facades (east, south, west) were segmented using the orthogonal projection of the corresponding cubicle wall. With this, the area to be analysed was the same on all three facades (9 m^2). To lessen the noise of the resulting clouds, a Statistical Outlier Removal (SOR) filter was

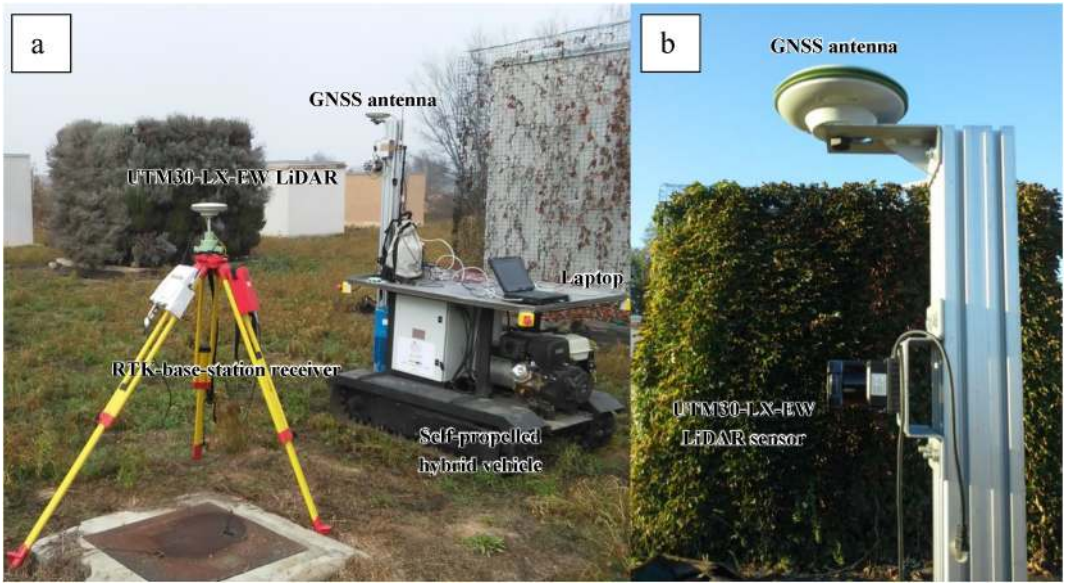


Fig. 6. a) General view of the MTLS performing a measurement of the double-skin green facade in winter, showing its main components. b) Detail of the UTM30-LX-EW LiDAR and the GNSS1200 + RTK-GNSS system.

Table 1
Characteristics of the MTLS system.

LiDAR sensor	Hokuyo UTM30-LX-EW
Light source	Laser semiconductor (class 1)
Wavelength	905 nm
Measurement range	0.1 m–30.0 m
Measurement accuracy	±30 mm (in the range 0.1–10 m)
Angular range	0°–270°
Angular resolution	0.25°
Scan rate	40 Hz
RTK-GNSS system	Leica GPS1200+
RTK-GNSS accuracy	10 mm (horizontal)/20 mm (vertical)
RTK-GNSS update rate	20 Hz

applied, considering the six nearest neighbouring points and a standard deviation equal to 1.

3. For the three green facades, the distance between each point of the cloud and the cubicle wall was computed.
4. The point clouds were rasterized, projecting each one on a plane parallel to its wall. Square cells were used in this process and the following cell sizes (cm) were evaluated: 5, 6.25, 8.33, 10, 12.5, 16.67, 20, 25, and 50. The scalar value of each pixel of the raster image was calculated as the average of the distances to the wall $\overline{d_{cw}}$ of all the points included in the cell associated with that pixel.
5. The cell volume (i.e., the vegetative volume corresponding to each cell) was estimated as the volume of a prism based on this cell:

$$V_c = s^2 \cdot \overline{d_{cm}} \quad \text{(Eq. 1)}$$

where s is the cell size (side length). $\overline{d_{cm}}$ is the average distance to the steel mesh of all the points included in the cell, and is given by:

$$\overline{d_{cm}} = \overline{d_{cw}} - d_{mw} \quad \text{(Eq. 2)}$$

$\overline{d_{cw}}$ being the average distance to the wall (step 4) and $d_{mw} = 25\ cm$ the separation between the wall and the mesh (Fig. 4). This method considers the vegetative volume that grows from the mesh outwards, neglecting the fraction of vegetation that grows inwards (towards the cubicle wall) (Fig. 7). As can be seen in Fig. 5d, the intermediate space between the steel mesh and the building facade wall remains free of leaves even in the periods of maximum plant development, so that this volume calculation estimate agrees with the fact that green facades grow mainly outwards.

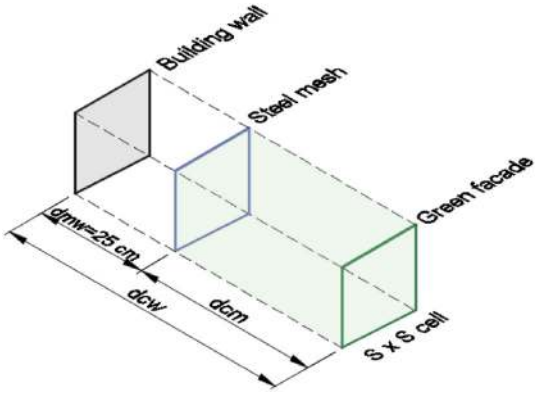


Fig. 7. Cell volume estimate.

6. Finally, the spatial distribution of vegetation on a facade depends on a number of factors, such as the hours of sunshine, how the different plants take root and the vigour of those plants. Sunshine affects the whole facade, while the other two factors may affect the width and/or height of the facade to different extents. This will be analysed by dividing the facades into three rows, each 1 m in height, and three columns, each 1 m in width. The intersection of rows and columns determine nine regions (Fig. 8). The vegetative volume of each facade, row, column or region was computed as the sum of all the cell volumes belonging to it. The processing of the results was carried out by facade, row, column and region.

Steps 1 to 3 of this processing were conducted using the software Cloud Compare (Cloud Compare [GPL software] v2.10.alpha), while MATLAB® (R2018a, Math Works Inc., Natick, Massachusetts, USA) was employed for point cloud generation and in processing steps 4 to 6.

2.3.3. Statistical analysis

A statistical analysis was applied with two purposes: (1) to study the repeatability of the system by comparing the two replicates, and (2) to

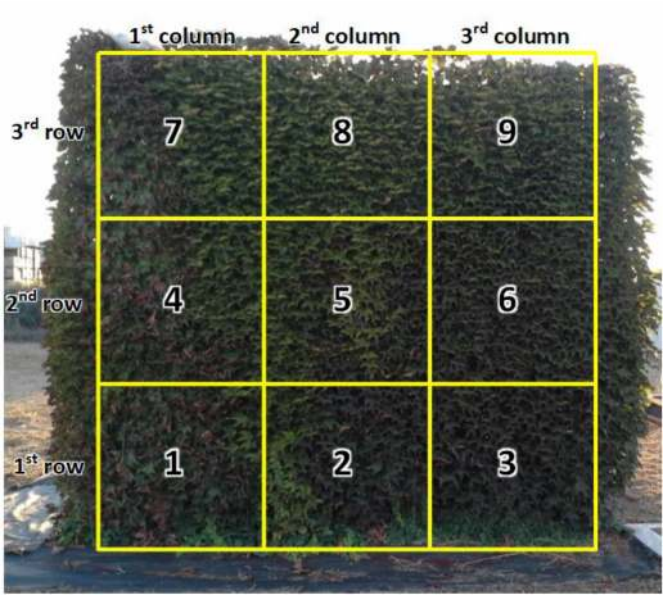


Fig. 8. Division of the green facade into regions (numbers within squares), rows and columns.

assess the differences in the vegetation's spatial distribution on the facades by comparing the average cell volume per facade, row, column and region.

The repeatability analysis consisted of comparing all the cell volumes on all three facades for each replicate and comparing the replicates of each facade. For this purpose, a factorial linear model with interaction was adjusted, considering the replicate and the facade as fixed factors and the cell volume as the dependent variable. An ANOVA was performed and the significance of the model was assessed. Then, the significance of each factor and the factors' interaction was observed. If the model was not significant, there was no reason to reject the null hypothesis and both replicates would be considered non-different as well as the average volumes of each facade. If the model was significant, the null hypothesis would be rejected and the significance of the factors as well as their interaction would be analysed. A Tukey honestly significant difference (HSD) test would be applied with a significance level of 0.05 to compare the mean cell volumes.

To assess the differences in vegetation distribution, a factorial linear model with interaction was adjusted for each facade, considering facade row and column as fixed factors. The significance of the model and of each factor was then assessed. If the effect of any of the factors were significant, the Tukey HSD test would be applied with a significance level of 0.05 to compare the mean cell volumes between rows, columns and possible interaction between these two factors, referring to the different regions on each facade. The statistical analyses were performed with JMP Pro 14.2.0. (SAS Institute Inc., Cary, NC, USA).

3. Results and discussion

3.1. 3D model of the green facade

Fig. 9 presents plan views of the cubicle generated from LiDAR measurements and corresponding to the no-vegetation case (Fig. 9a) and to the completely developed greenery (Fig. 9b). The solid white line indicates the position of the cubicle wall (GNSS points: FV1, FV2, FV3 and FV4), while the dashed white line marks the position of the steel mesh (GNSS points: FV5, FV6, FV7 and FV8). The growth of the vegetation is evidenced by comparing both views. When there is no vegetation (Fig. 9a), the LiDAR sensor measures the cubicle wall. With the presence of vegetation (Fig. 9b), the laser beam is not able to reach the wall and the outer enveloping of the vegetation is scanned.

From these measurements it was possible to rebuild the point cloud that characterizes the double-skin green facade vegetation volume at its maximum development. Fig. 10 shows a 3D reconstruction of the cubicle with completely developed vegetation.

In Wong and Zhou [15] the future lines of research towards "Green BIM" adoption in the building sector were settled. In addition, the importance of extending the application of cloud computing and managing big data in green BIM was highlighted. By obtaining the volume of the green facade under study, the authors have contributed to the achievement of this innovative research trend within the building and architecture sector.

However, clearly there is still a lack of research in this direction and only a few similar cases can be found, for example those where the concept of "scan-to-BIM" is defined to compare the as-built data of construction projects with the planned works [59].

In the case of construction systems where vegetation can be integrated into the building envelope, these technologies are even more

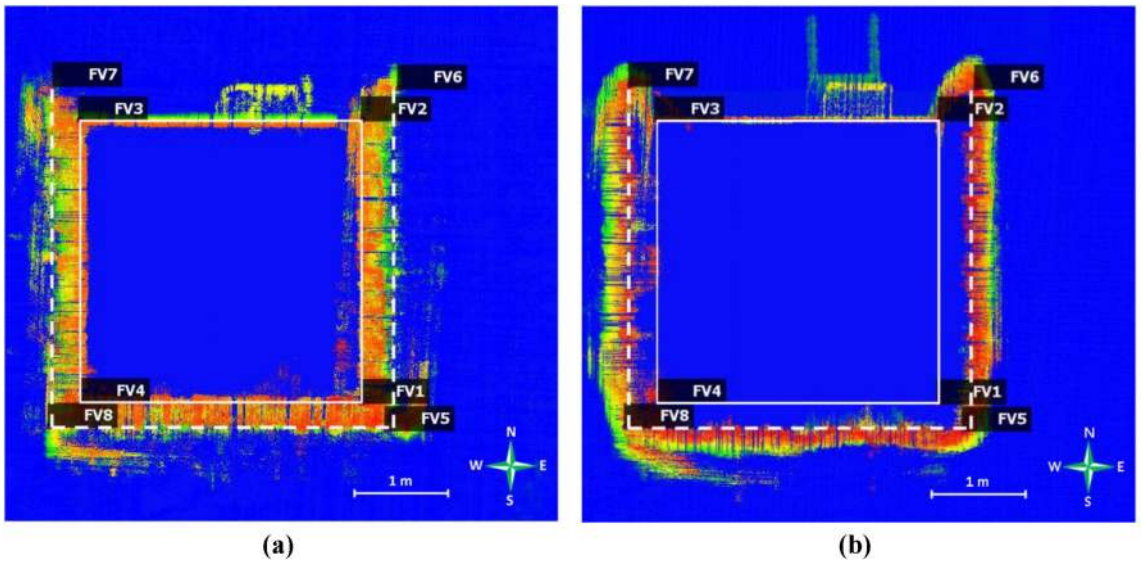


Fig. 9. Plan view detail of the cubicle with the double-skin facade: (a) without vegetation in winter (December); (b) with completely developed vegetation in late summer (September).

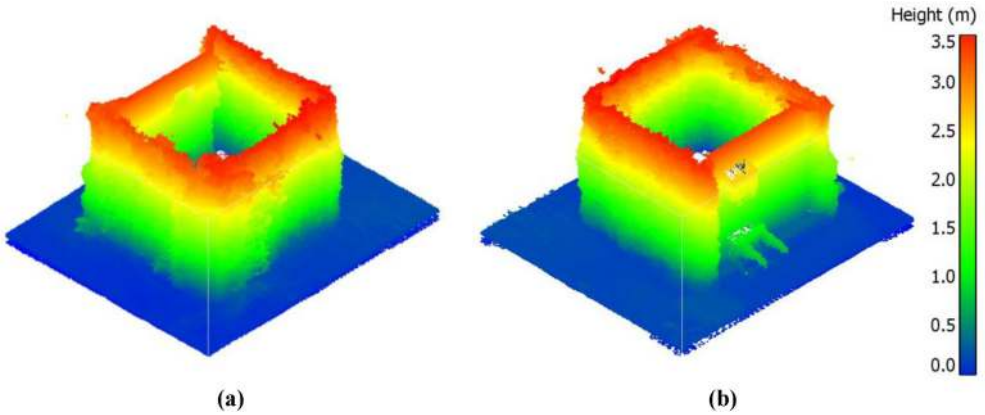


Fig. 10. 3D view of the point cloud generated by the LiDAR sensor with completely developed vegetation: (a) south/west facades; (b) north/east facades. The colours refer to the height of the points, the blue ones being those at ground level. (For interpretation of the references to colour in this figure legend, the reader is referred to the Web version of this article.)

interesting to study, as the level of variation and heterogeneity of organic shapes and volumes is higher than typical inert construction elements.

3.2. Comparison between facades and analysis of the precision of the system

Current state-of-the-art technology presents several methods for estimating vegetative volume from point clouds, either by adjusting simple geometric bodies (cubes, cylinders, trapezoids, etc.) or through computational geometry (convex-hull, alpha-shape, voxelization, etc.) [60–62]. Although these methods make it possible to estimate the volume of porous vegetative structures (e.g. the crown volume of a tree), they are not appropriate for determining the volume of a completely developed green facade such as the one assessed in this work. Due to its high foliar density, the laser beams emitted by the LiDAR system collided with the outer layers of the vegetated facade. For this reason, the resulting point cloud cannot be considered a 3D image of the entire vegetative volume, but rather a reconstruction of its outer envelope. The method proposed in this work is based on determining the volume between the envelope and the steel mesh. Fig. 11 shows the estimated volume of vegetation for each facade orientation and for each replicate considering different cell sizes. It can be observed that, with this method, the volume of vegetation remains almost constant regardless of the cell size.

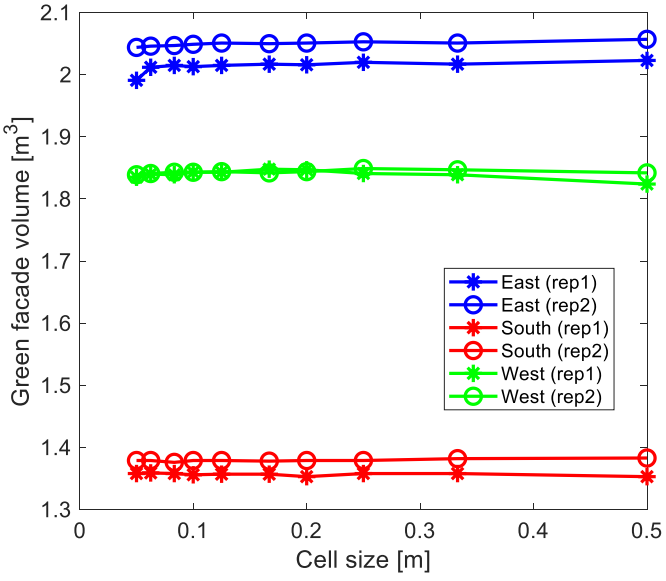


Fig. 11. Vegetation volume on each facade (replicates 1 and 2) for several cell sizes.

A cell size of 10 cm has been considered in the analysis that follows. This is the minimum size for which no empty cells (no LiDAR points) are obtained on all facades and for all replicates. The vegetation volume was computed by adding the volume of the considered individual cells (full facade, by rows, by columns or by regions).

The factorial linear model adjusted to all the data (N = 5400) to analyse the effect of the factors Replicates and Facade Orientation resulted significant (p-value < 0.0001). However, the effect of the Replicate factor was not significant (p-value = 0.2067). Thus, there is no evidence to reject the null hypothesis, so we can consider there are no significant differences between the two replicates. The total cell unit volume average for rep 1 is 1.930 dm^3 while for rep 2 it is 1.952 dm^3 ($N_{rep\ 1} = N_{rep\ 2} = 2700$). The effect of the Facade Orientation factor was significant (p-value < 0.0001), but the interaction with the Replicates was not (p-value = 0.6384). Hence, while differences were found between facades, no significant differences were found between replicates within each facade. The results are presented in Table 2.

The per-facade average cell volume does not present statistically significant differences between replicates. However, there are clear differences between facade averages (Table 2). The facade orientation with higher average cell volume and, hence, with higher total volume, is the east facade, followed by the west and south ones. The variability in

Table 2
Comparison between facades and replicates (rep i) of the vegetation volume per facade orientation (cell size = 10 cm), number of LiDAR points, number of cells, average cell volume (averages not connected by the same letter are significantly different according to the Tukey HSD test (α = 0.05)) and standard deviation.

Parameter	East (rep 1)	East (rep 2)	South (rep 1)	South (rep 2)	West (rep 1)	West (rep 2)
Total volume [m^3]	2.013	2.049	1.356	1.379	1.843	1.843
Number of LiDAR points	101456	123838	116097	119276	116339	117283
Number of cells	900	900	900	900	900	900
Average cell volume [dm^3]	2.236a	2.277a	1.506c	1.532c	2.047b	2.048b
Standard deviation [dm^3]	0.487	0.459	0.575	0.579	0.819	0.829

cell volumes is lower in the east facade, followed by the south and west ones. This is clearly seen in Fig. 12.

The vegetation distribution on each facade is described and analysed in the following sections. As no significant differences are found between replicates, the following results refer to rep 1.

These results perfectly reflect the development of vegetation on each facade. The variation in the results obtained on different facades illustrates the influence of microclimate on plant development. Thus, in this specific location there is a constant south-westerly breeze, which slows the growth of vegetation on these two facades. This fact has already been observed in previous studies to characterize leaf density, using traditional techniques for measuring the LAI [10,14]. In the case of the eastern facade, which is more protected from the local dominant breeze, year after year the vegetation generally has a higher growth, which was well characterized in the largest volume recorded.

As for the difference in volume between the south and west facades, although in a normal year these orientations reach a similar volume, at the time of the 3D data gathering, a couple of plants located on the left zone of the south facade were suffering from a disease that decreased the number and volume of the leaves and consequently the total volume of this facade orientation. For this reason, a lower volume of 1.356 m^3 (rep 1) was measured on the south facade as compared to the 1.843 m^3 (rep 1) reached on the west facade.

3.3. Per-facade vegetation volume analysis

The distribution of the vegetation on each facade is commented and analysed in the following sections. Visual representations of its spatial distribution are shown in Figs. 13–15. A multifactorial linear model was adjusted to the rep 1 data (N = 2700) to assess the effect of factors Row and Column and their interaction on each facade. Results are presented in Tables 3–5.

3.3.1. East facade

As shown in Fig. 13, the spatial distribution of vegetation on the east facade is not uniform. The vegetation depth ranges from 30 cm to more than 60 cm with a decreasing pattern in height. The results of the statistical analysis prove the significance of factors Row and Column and of their interaction (all p-values < 0.0001). What and where are the differences in Table 3. When analysing the rows or columns individually, it is possible to obtain a rough approach to the real situation. For example, columns 2 and 3 have significantly higher cell volume averages than column 1. Moreover, the average cell volume in row 1 is significantly higher than it is in row 2 and row 3. However, this is not entirely true for the entire height of the column or length of the row. Thus, the least vegetated region is region 7, closely followed by regions 8, 9, 4 and 1. The most vegetated regions are regions 2 and 3, followed by regions 6 and 5. It is reasonable to have more vegetation close to the roots of the plants with a decreasing pattern in height, and that is clearly seen in the row results.

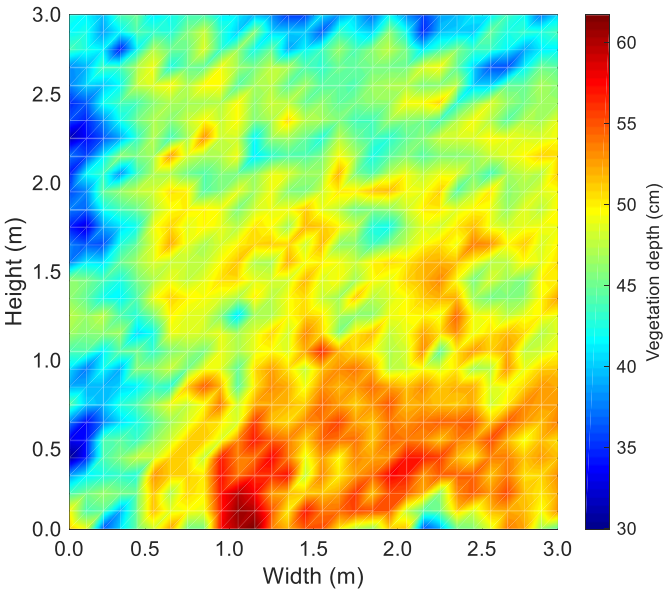


Fig. 13. East facade. The colour scale indicates the vegetation depth (i.e. distance of the vegetation from the wall). (For interpretation of the references to colour in this figure legend, the reader is referred to the Web version of this article.)

Differences in columns can usually be explained when some plants are less vigorous than others. That happens when plants are not properly rooted or when soil properties are variable along the facade width. However, in the case of this east facade, the lower volume in column 1 was the consequence of a disease that mainly affected the plants located in the southeast corner that took place at the time of the measurements. This fact not only implied a decrease in the volume of columns 2 and 3 of the south facade but also affected column 1 of this east facade as can be clearly observed in Fig. 13.

This event was specific to the year and time of the data collection and after this disease the plants again recovered normally. This fact highlights, on the one hand, the influence that a disease can have on the vegetation volume and consequently on the ability to produce shade and provide energy savings during the cooling period, and on the other hand, as previous authors have highlighted, the importance of maintenance operations when vertical greening systems are used [4].

3.3.2. South facade

Fig. 14 shows the high variability of the south facade, with vegetation depth ranging from 15 cm to 55 cm. Visual observation shows low vegetation development in regions 3 and 9, and in region 6 to a lesser

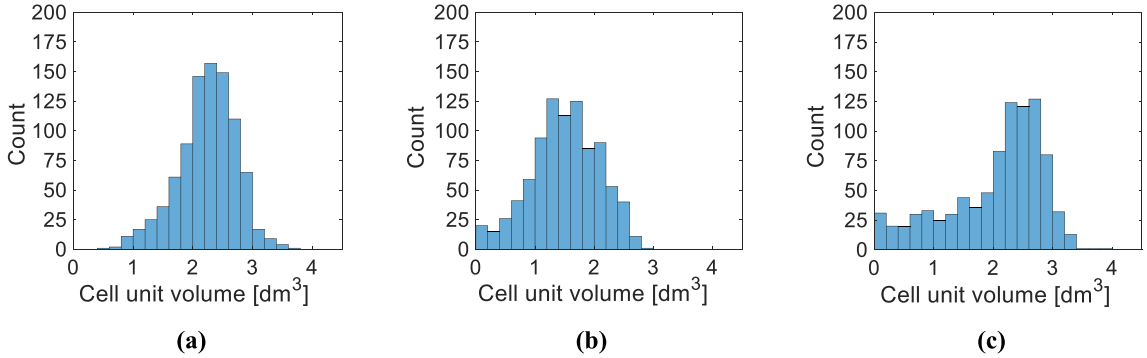


Fig. 12. Vegetation volume distribution histograms. Count (vertical) vs. cell unit volume (horizontal) for the three facades: (a) east (N = 900); (b) south (N = 900); (c) west (N = 900).

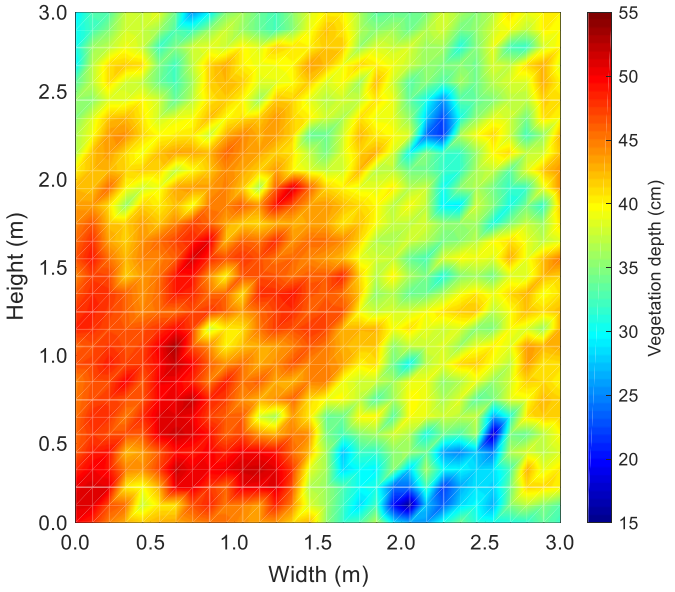


Fig. 14. South facade. The colour scale indicates the vegetation depth (i.e. distance of the vegetation from the wall). (For interpretation of the references to colour in this figure legend, the reader is referred to the Web version of this article.)

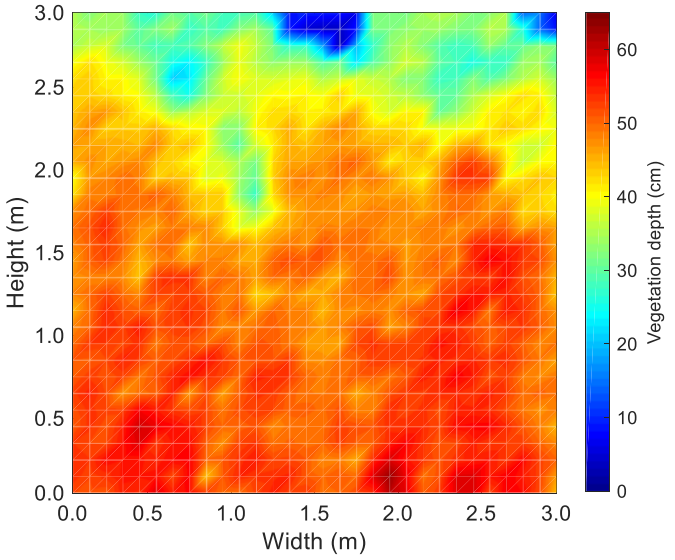


Fig. 15. West facade. The colour scale indicates the vegetation depth (i.e. distance of the vegetation from the wall). (For interpretation of the references to colour in this figure legend, the reader is referred to the Web version of this article.)

extent. It is confirmed through statistical analysis, where the effects of factors Row and Column, and their interaction, proved to be significant (all p-values < 0.0001). The average cell volume in column 3 is significantly lower than in columns 1 and 2 (Table 4). Row total average cell volumes 1 and 3 are also significantly lower than row 2. However, the most vegetated zone is region 1.

As previously mentioned, at the time of the measurement, a disease was affecting the plants in columns 2 and 3 of the south facade, which temporarily reduced their volume. This fact was perfectly captured during the data collection process as shown in Fig. 14, highlighting the effectiveness of the set methodology as well as the data collection process.

As on the other facades, the volume is always higher in the lower rows than in the upper ones, coinciding with the logical growth of the plants. This fact was already characterized in previous LAI measurement studies using traditional methods [10,14]. Perhaps in future experiments it would be necessary to study in detail how this volume decrease with the plant height influences the ability to provide shade and energy savings for cooling.

Table 3
Vegetation volume [m^3] on east facade according to the different regions, rows ($N_{row\ i} = 300$) and columns ($N_{col\ i} = 300$) with their totals.

	Column 1	Column 2	Column 3	Row Totals
Row 3	0.185 (1.849d)	0.196 (1.957cd)	0.199 (1.987cd)	**0.579 (1.931δ)**
Row 2	0.204 (2.042c)	0.236 (2.364b)	0.244 (2.438b)	**0.684 (2.282χ)**
Row 1	0.208 (2.076c)	0.279 (2.790a)	0.263 (2.625a)	**0.749 (2.497β)**
Column Totals	**0.597 (1.989B)**	**0.711 (2.371A)**	**0.705 (2.350A)**	**2.013 (2.237)**

Average cell volumes [dm^3] are included in brackets. Averages not connected by the same lowercase letters are significantly different. Column total averages not connected by the same uppercase letters are significantly different. Row total averages not connected by the same Greek letters are significantly different. All average comparisons applied the Tukey HSD test ($\alpha = 0.05$).

Table 4
Vegetation volume [m^3] on south facade according to the different regions, rows ($N_{row\ i} = 300$) and columns ($N_{col\ i} = 300$), with their totals.

	Column 1	Column 2	Column 3	RowTotals
Row 3	0.130 (1.300def)	0.141 (1.412de)	0.112 (1.118fg)	**0.383 (1.276δ)**
Row 2	0.200 (2.002b)	0.182 (1.816c)	0.127 (1.267ef)	**0.509 (1.695β)**
Row 1	0.222 (2.217a)	0.147 (1.468d)	0.096 (0.958g)	**0.464 (1.548χ)**
Col Totals	**0.552 (1.840A)**	**0.470 (1.565B)**	**0.334 (1.114C)**	**1.356 (1.506)**

Average cell volumes [dm^3] are included in brackets. Averages not connected by the same lowercase letters are significantly different. Column total averages not connected by the same uppercase letters are significantly different. Row total averages not connected by the same Greek letters are significantly different. All average comparisons applied the Tukey HSD test ($\alpha = 0.05$).

Table 5
Vegetation volume [m^3] on west facade according to the different regions, rows ($N_{row\ i} = 300$) and columns ($N_{col\ i} = 300$) with their totals.

	Column 1	Column 2	Column 3	Row Totals
Row 3	0.121 (1.209e)	0.114 (1.136e)	0.107 (1.072e)	**0.342 (1.139δ)**
Row 2	0.234 (2.342cd)	0.216 (2.157d)	0.241 (2.410bc)	**0.691 (2.303χ)**
Row 1	0.275 (2.752a)	0.260 (2.603ab)	0.275 (2.746a)	**0.810 (2.701β)**
Col Totals	**0.630 (2.101A)**	**0.590 (1.966B)**	**0.623 (2.076A)**	**1.843 (2.048)**

Average cell volumes [dm^3] are included in brackets. Averages not connected by the same lowercase letters are significantly different. Column total averages not connected by the same uppercase letters are significantly different. Row total averages not connected by the same Greek letters are significantly different. All average comparisons applied the Tukey HSD test ($\alpha = 0.05$).

3.3.3. *West facade*

The west facade looks much more uniform than the other two (Fig. 15). Although the adjusted factorial model was significant, the significance of factors Row (p-value < 0.0001), Column (p-value $= 0.0011$) and their interaction (p-value $= 0.0199$) was slightly lower.

As on the other facade, the rows on this west facade follow a

significantly decreasing pattern in height, which clearly characterizes the vertical growth of plants (Table 5). Differences between columns are small, although significant.

In this case, the smaller volumes recorded in row 3, especially in columns 2 and 3 (regions 8 and 9), are explained by the influence of the breeze that constantly impacts in a southwest direction and clearly hinders the growth of plants in height. This fact has been verified by many years of experimentation [10,14], and it was also reflected in the current study on the geometrical description and calculation of green facade volume.

3.4. Relationship between vegetation volume and shadow effect

Although the main objective of this study was the geometrical characterization of the green facade and not the evaluation of the shadow effect and its connotations in energy savings, there is a close relationship between these topics that it is worth discussing.

In complementary previous studies, the measurement of the leaf density of the same double-skin green facade was characterized using the Leaf Area Index (LAI), both by the direct method (destructive) and by the indirect method (using appropriate equipment e.g. ceptometer) [14]. Moreover, a per-facade orientation analysis of the double-skin green facade's contribution to passive energy savings was also conducted [10]. On Summer 2015, with a higher foliage development, the positive thermal behaviour of this green facade was confirmed by representative reductions on the external surface wall temperature in all orientations (East, South and West). In addition, tests under controlled temperatures showed the high potential of the double-skin green facade as a passive system in comparison to the reference one, obtaining accumulated electrical energy savings up to 34% for cooling periods with a LAI of 3.5–4 during the Summer period, under Mediterranean continental climate [10,14].

Although no measurements about the energy performance were conducted during the research presented in this paper, the development of the green facade was quite similar than during those previous energy experiments, since once plants reach maturity, their development is quite similar each new summer season. On the basis of this premise, in this section the main goal is look for a correspondence between the measured volume and the obtained results from the previous energy experimentation.

To conduct this comparative, it should be remembered that in previous studies it was determined that the most interesting parameter for quantifying the contribution of VGS to passive energy savings in buildings is the reduction of the external surface temperature of the building facade wall (ΔT parameter). Using this parameter as a reference, it is possible to compare research studies regardless of the facade construction system used on the building [9].

Since the external surface temperature probe on the building facade wall during energy experiments [10,14] was located at the central point of the facade, it is considered that the vegetation volumes, achieved in region 5 are decisive in the evolution of these surface temperatures during the cooling period (summer).

Table 6 shows the vegetation volumes for region 5 by orientation, as well as the average external wall surface temperature reduction achieved, expressed as ΔT (°C).

Regarding the reductions obtained in the external surface temperature as a consequence of the existence of the green facade, the correspondence between the volume of vegetation measured in the present study and the measured reductions for studies on energy savings from the same green facade can be observed.

Table 6
Relationship between measured volume in region 5 and external surface temperature reductions in [10].

Orientation/ Region	Measured vegetation volume (rounded value) (m^3)	Average reduction ΔT (°C) [10]
East 5	0.24	**−13.8**
South 5	0.18	**−10.7**
West 5	0.22	**−13.9**

These results are very encouraging because they not only show that the methodology used to measure the volume of vegetation was appropriate but they also open a very interesting path for research in terms of connecting the data on shadow effect and energy savings with the shape geometry of the green facade. Generalizing the values obtained from these research studies, it could be concluded that with vegetation volumes of 0.2 m^3/m^2, reductions in external building surface temperatures (ΔT parameter) of 13 °C can be obtained. Thus, this data could be used in the future in the design of BIM objects for green facades, specifically in the definition of the analytical properties of the BIM object, allowing them to be used in energy simulations based on the 3D model of the building to which the green construction systems may be applied.

4. Conclusions

The growing use of BIM objects in the processes of design and simulation of building's behaviour (thermal, acoustic, etc.), has generated the need to improve the geometric representation and the incorporated information in the objects related to the urban green infrastructure, and especially those construction systems integrated into the building envelope, such as roofs and green facades.

Given the difficulty of geometrically characterizing vegetation, the few examples of 3D objects relating to building-integrated vegetation systems tend to oversimplify shapes and not to incorporate any parameter (information) regarding their behaviour as a passive tool for energy saving. A first step towards the normalization of this situation is the 3D characterization of the real cases volumes, in the same way that it is being done in other disciplines, such as precision agriculture.

In this research, the characterization of a double-skin green facade using an MTLS typically applied in precision agriculture, in order to obtain a reliable three-dimensional representation of the foliage, was conducted.

From the results, the following main conclusions can be drawn:

- The proposed capture methodology has proven to be precise and robust. There were no significant differences between the two replications carried out during the point cloud capture process using the LiDAR sensor, thus enabling the further 3D reconstruction of the green facade's outer envelope.
- The suggested volume calculation methodology, based on determining the volume between the envelope and the steel mesh, was also appropriate.
- Significant volume differences were found between the different facade orientations, reaching values of 2 m^3 on the east orientation (more protected from local breezes), 1.4 m^3 on the south side (influenced by a constant breeze and a disease in the left zone of the facade), and 1.8 m^3 on the west side (influenced by a constant breeze). This fact highlights the influence of cardinal direction and local microclimate on the final development of the plants.
- Differences in height were found, the facade being more voluminous in all directions on the bottom regions closer to the base of the plants and less voluminous in higher areas (growth zones), away from the roots.
- The differences between rows within a side can be explained by the local microclimate (the south-westerly breeze) and the impact of specific diseases, in this case in the southeast corner. In addition to the local microclimate, plant maintenance also stands out as a key contributor to the ability of plants to provide ecosystem services (shadow effect).
- From this research, together with complementary previous research, it could be concluded that, generally speaking, with vegetation

volumes of 0.2 m^3/m^2, reductions in external building surface temperatures of 13 °C can be reached.

The results and conclusions of this research pave the way for the future definition of BIM objects for green facades and green walls, to which it could be possible to incorporate analytical parameters that would make it possible to simulate their contribution not only to energy savings but also to other ecosystem services during the architectural project phase. Future research could address this issue, so that the point clouds of green systems obtained following the methodology defined in this research can be arranged and inserted using the appropriate BIM software to create the BIM objects.

This process will be crucial to ensure that all these nature-based construction systems (green infrastructure), which make the integration of vegetation into building envelopes possible, can be considered during the early stages of architectural design, which usually include simulations of building performance, in the same conditions as conventional (grey infrastructure) solutions are.

The present work has to be understood as an initial step towards the geometric characterization of green facades which should be complemented with further studies considering different species and alternative 3D sensors. In this regard, there is a clear parallelism with the precision agriculture area, where the use of LiDAR sensors has allowed the geometric and structural characterization of tree-row crops and estimate canopy parameters whose knowledge allows the farmer to optimize the agricultural inputs. Similarly, future studies should analyse potential relationships between the geometric parameters of the green facade (derived from 3D sensor measurements) and its environmental capacity (thermal and acoustic insulation, evaporative cooling, pollution capture and CO_2 sequestration, etc.).

Declaration of competing interest

The authors declare that they have no known competing financial interests or personal relationships that could have appeared to influence the work reported in this paper.

Acknowledgements

The authors at GREiA research group would like to thank the Catalan Government for the quality accreditation given to their research group (2017 SGR 1537). GREiA is a certified agent TECNIO in the category of technology developers from the Government of Catalonia. The authors at GRAP research group would like to thank the Secretaria d'Universitats i Recerca del Departament d'Empresa i Coneixement de la Generalitat de Catalunya (grant 2017 SGR 646), the Spanish Ministry of Economy and Competitiveness (project AGL2013-464 48297-C2-2-R) and the Spanish Ministry of Science, Innovation and Universities (project RTI2018-094222-B-I00). This work is partially supported by ICREA under the ICREA Academia programme. The authors also wish to thank Dr. Jaume Arnó for his contribution in the statistical analysis of the results.

References

[1] World Population Prospects, United nations. Department of economic and social affairs. Population division. https://population.un.org/wpp.
[2] Urban and rural population projected to 2050, World. Global Change Data Lab. Oxford Martin Programme on Global Development at the University of Oxford. Based on Urban population long-run with 2050 projections (OWID) data. https://ourworldindata.org/.
[3] Division for sustainable development goals (DSDG) in the united nations department of economic and social affairs (UNDESA). https://sustainabledevelopment.un.org/sdg11.
[4] G. Pérez, K. Perini, Nature Based Strategies for Urban and Building Sustainability, Elsevier, 2018, https://doi.org/10.1016/C2016-0-03181-9. Imprint: Butterworth-Heinemann. eBook ISBN: 9780128123249. Paperback ISBN: 9780128121504.
[5] Y. Wang, F. Bakker, R. de Groot, H. Wörtche, Effect of ecosystem services provided by urban green infrastructure on indoor environment: a literature review, Build. Environ. 77 (2014) 88–100, https://doi.org/10.1016/j.buildenv.2014.03.021.
[6] T. Matthews, A.Y. Lo, J.A. Byrne, Reconceptualizing green infrastructure for climate change adaptation: barriers to adoption and drivers for uptake by spatial planners, Landsc. Urban Plann. 138 (2015) 155–163, https://doi.org/10.1016/j.landurbplan.2015.02.010.
[7] H. Saaroni, J.H. Amorim, J.A. Hiemstra, D. Pearlmutter, Urban Green Infrastructure as a tool for urban heat mitigation: survey of research methodologies and findings across different climatic regions, Urban Clim 24 (2018) 94–110, https://doi.org/10.1016/j.uclim.2018.02.001.
[8] E. Alexandri, P. Jones, Temperature decreases in an urban canyon due to green walls and green roofs in diverse climates, Build. Environ. 43 (4) (2008) 480–493, https://doi.org/10.1016/j.buildenv.2006.10.055.
[9] G. Pérez, J. Coma, I. Martorell, L.F. Cabeza, Vertical Greenery Systems (VGS) for energy saving in buildings: a review, Renew. Sustain. Energy Rev. 39 (2014) 139–165, https://doi.org/10.1016/j.rser.2014.07.055.
[10] J. Coma, G. Pérez, A. de Gracia, S. Burés, M. Urrestarazu, L.F. Cabeza, Vertical greenery systems for energy savings in buildings: a comparative study between green walls and green facades, Build. Environ. 111 (2017) 228–237, https://doi.org/10.1016/j.buildenv.2016.11.014.
[11] G. Pérez, L. Rincón, A. Vila, J.M. González, L.F. Cabeza, Behaviour of green façades in Mediterranean Continental climate, Energy Convers. Manag. 52 (2011) 1861–1867, https://doi.org/10.1016/j.enconman.2010.11.008.
[12] C.Y. Jim, Thermal performance of climber greenwalls: effects of solar irradiance and orientation, Appl. Energy 154 (2015) 631–643, https://doi.org/10.1016/j.apenergy.2015.05.077.
[13] G. Pérez, L. Rincón, A. Vila, J.M. González, L.F. Cabeza, Green vertical systems for buildings as passive systems for energy savings, Appl. Energy 88 (2011) 4854–4859, https://doi.org/10.1016/j.apenergy.2011.06.032.
[14] G. Pérez, J. Coma, S. Sol, L.F. Cabeza, Green facade for energy savings in buildings: the influence of leaf area index and façade orientation on the shadow effect, Appl. Energy 187 (2017) 424–437, https://doi.org/10.1016/j.apenergy.2016.11.055.
[15] J.K.W. Wong, J. Zhou, Enhancing environmental sustainability over building life cycles through green BIM: a review, Autom. ConStruct. 57 (2015) 156–165, https://doi.org/10.1016/j.autcon.2015.06.003.
[16] S. Sevis, Mixed method review for integrating building information modeling and life-cycle assessments, Build. Environ. 173 (2020) 106703, https://doi.org/10.1016/j.buildenv.2020.106703.
[17] M. Najjar, K. Figueiredo, M. Palumbo, A. Haddad. Integration of BIM and LCA: evaluating the environmental impacts of building materials at an early stage of designing a typical office building, J. Build. Eng. 14 (2017) 115–126, https://doi.org/10.1016/j.jobe.2017.10.005.
[18] M. Ignatius, N.H. Wong, M. Martin, S. Chen. Virtual Singapore integration with energy simulation and canopy modelling for climate assessment. IOP Conference Series: Earth and Environmental Science, Volume 294, Sustainable Built Environment Conference 2019 Tokyo (SBE19Tokyo) Built Environment in an Era of Climate Change: How Can Cities and Buildings Adapt? 6–7 August 2019, The University of Tokyo, Japan https://doi.org/10.1088/1755-1315/294/1/012018.
[19] S. Chen, K. Lok, T. Jeng, Smart BIM object for design intelligence. 21st international conference on computer-aided architectural design research in asia: living systems and micro-utopias: towards continuous designing, CAADRIA 2016, Melbourne, Australia. ISBN (Electronic): 9789881902672, https://researchoutput.ncku.edu.tw/en/publications/smart-bim-object-for-design-intelligence.
[20] J. Wang, W. Lu, D. Liu, F. Xue, The heterogeneity of BIM objects in different construction contexts, Construction Research Congress (2018) 210–220, https://doi.org/10.1061/9780784481264.021.
[21] R. Miettinen, S. Paavola, Beyond the BIM utopia: approaches to the development and implementation of building information modelling, Autom. ConStruct. 43 (2014) 84–91, https://doi.org/10.1016/j.autcon.2014.03.009.
[22] G. Perez, J. Coma, J. Barrau. Green walls 3D modelling. 14th Conference on Advanced Building Skins. 28-29 October 2019. Bern, Switzerland. ISBN: 978-3-9524883-0-0 https://abs.green/files/pdf/content-2019.pdf.
[23] J.A.C. Castellar, L.A. Popartan, J. Pueyo-Ros, N. Atanasova, G. Langergraber, I. Säumel, L. Corominas, J. Comasa, V. Acuña, Nature-based solutions in the urban context: terminology, classification and scoring for urban challenges and ecosystem services, Sci. Total Environ. 779 (2021) 146237, https://doi.org/10.1016/j.scitotenv.2021.146237.
[24] bimobject library. https://www.bimobject.com/en/product?sort=trending.
[25] NBS National BIM Library. https://www.nationalbimlibrary.com/en/.
[26] G. Pérez, J. Coma, C. Barreneche, A. De Gracia, M. Urrestarazu, S. Burés, L. F. Cabeza, Acoustic insulation capacity of vertical greenery systems for buildings, Appl. Acoust. 110 (2016) 218–226, https://doi.org/10.1016/j.apacoust.2016.03.040.
[27] L. Barazzetti, F. Banfi, R. Brumana, M. Previtali, Creation of parametric BIM objects from point clouds using Nurbs, Photogramm. Rec. 30 (152) (2015) 339–362, https://doi.org/10.1111/phor.12122.
[28] J.R. Rosell, R. Sanz, A review of methods and applications of the geometric characterization of tree crops in agricultural activities, Comput. Electron. Agric. 81 (2012) 124–141, https://doi.org/10.1016/j.compag.2011.09.007.
[29] J.R. Rosell Polo, R. Sanz, J. Llorens, J. Arnó, A. Escolà, M. Ribes-Dasi, J. Masip, F. Camp, F. Gràcia, F. Solanelles, T. Pallejà, L. Val, S. Planas, E. Gil, J. Palacín, A tractor-mounted scanning LIDAR for the non-destructive measurement of vegetative volume and surface area of tree-row plantations: a comparison with conventional destructive measurements, Biosyst. Eng. 102 (2) (2009) 128–134, https://doi.org/10.1016/j.biosystemseng.2008.10.009.

[30] A. Escolà, J.A. Martínez-Casasnovas, J. Rufat, J. Arnó, A. Arbonés, F. Sebé, M. Pascual, E. Gregorio, J.R. Rosell-Polo, Mobile terrestrial laser scanner applications in precision fruticulture/horticulture and tools to extract information from canopy point clouds, Precis. Agric. 18 (1) (2017) 111–132, https://doi.org/10.1007/s11119-016-9474-5.
[31] E. Gil, J. Arnó, J. Llorens, R. Sanz, J. Llop, J.R. Rosell-Polo, M. Gallart, A. Escolà, Advanced technologies for the improvement of spray application techniques in Spanish viticulture: an overview, Sensors 14 (1) (2014) 691–708, https://doi.org/10.3390/s140100691.
[32] V. Méndez, J.R. Rosell-Polo, R. Sanz, A. Escolà, H. Catalán, Deciduous tree reconstruction algorithm based on cylinder fitting from mobile terrestrial laser scanned point clouds, Biosyst. Eng. 124 (2014) 78–88, https://doi.org/10.1016/j.biosystemseng.2014.06.001.
[33] J. Gené-Mola, E. Gregorio, F. Auat, J. Guevara, J. Llorens, R. Sanz-Cortiella, A. Escolà, J.R. Rosell-Polo, Fruit detection, yield prediction and canopy geometric characterization using LiDAR with forced air flow, Comput. Electron. Agric. 168 (2020) 105121, https://doi.org/10.1016/j.compag.2019.105121.
[34] J.R. Rosell, J. Llorens, R. Sanz, J. Arnó, M. Ribes-Dasi, J. Masip, A. Escolà, F. Camp, F. Solanelles, F. Gràcia, E. Gil, L. Val, S. Planas, J. Palacín, Obtaining the three-dimensional structure of tree orchards from remote 2D terrestrial LIDAR scanning, Agric. For. Meteorol. 149 (9) (2009) 1505–1515, https://doi.org/10.1016/j.agrformet.2009.04.008.
[35] R. Sanz-Cortiella, J. Llorens-Calveras, A. Escolà, J. Arnó-Satorra, M. Ribes-Dasi, J. Masip-Vilalta, F. Camp, F. Gràcia-Aguilà, F. Solanelles-Batlle, S. Planas-DeMartí, T. Pallejà-Cabré, J. Palacin-Roca, E. Gregorio-López, I. Del-Moral Martínez, J. R. Rosell-Polo, Innovative LIDAR 3D dynamic measurement system to estimate fruit-tree leaf area, Sensors 11 (6) (2011) 5769–5791, https://doi.org/10.3390/s110605769.
[36] P.R.W. Urech, M.A. Dissegna, C. Girot, A. Grêt-Regameya, Point cloud modeling as a bridge between landscape design and planning, Landsc. Urban Plann. 203 (2020) 103903, https://doi.org/10.1016/j.landurbplan.2020.103903.
[37] M. Kulawiak, Z. Lubniewski, Improving the accuracy of automatic reconstruction of 3D complex buildings models from airborne Lidar point clouds, Rem. Sens. 12 (10) (2020) 1643, https://doi.org/10.3390/rs12101643.
[38] C. Wang, N. Fareed, Mapping drainage structures using airborne laser scanning by incorporating road centerline information, Rem. Sens. 13 (3) (2021) 463, https://doi.org/10.3390/rs13030463.
[39] M. Somrak, S. Dzeroski, Z. Kokalj, Learning to classify structures in ALS-derived visualizations of ancient Maya settlements with CNN, Rem. Sens. 12 (14) (2020) 2215, https://doi.org/10.3390/rs12142215.
[40] M. Bisson, A. Tadini, R. Gianardi, A. Angioletti, The use of historical cartography and ALS technology to map the geomorphological changes of volcanic areas: a case study from Gran Cono of Somma-Vesuvius volcano, Geomorphology 380 (2021) 107624, https://doi.org/10.1016/j.geomorph.2021.107624.
[41] E. Heinaro, T. Tanhuanpää, T. Yrttimaa, M. Holopainen, M. Vastaranta, Airborne laser scanning reveals large tree trunks on forest floor, For. Ecol. Manag. 491 (2021) 119225, https://doi.org/10.1016/j.foreco.2021.119225.
[42] M. Michalowska, J. Rapinski, A review of tree species classification based on airborne LiDAR data and applied classifiers, Rem. Sens. 13 (3) (2021) 353, https://doi.org/10.3390/rs13030353.
[43] Z. Muszyński, M. Wyjadłowski, Assessment of the shear strength of pile-to-soil interfaces based on pile surface topography using laser scanning, Sensors 19 (5) (2019) 1012, https://doi.org/10.3390/s19051012.
[44] R. Maalek, D. D Lichti, J.Y. Ruwanpura, Robust segmentation of planar and linear features of terrestrial laser scanner point clouds acquired from construction sites, Sensors 18 (3) (2018) 819, https://doi.org/10.3390/s18030819.
[45] L. Yuan, J. Guo, Q. Wang, Automatic classification of common building materials from 3D terrestrial laser scan data, Autom. ConStruct. 110 (2020) 103017, https://doi.org/10.1016/j.autcon.2019.103017.
[46] Y. Yin, J. Antonio, Application of 3D laser scanning technology for image data processing in the protection of ancient building sites through deep learning, Image Vis Comput. 102 (2020) 103969, https://doi.org/10.1016/j.imavis.2020.103969.
[47] H. El-Din Fawzy, 3D laser scanning and close-range photogrammetry for buildings documentation: a hybrid technique towards a better accuracy, Alex. Eng. J. 58 (4) (2019) 1191–1204, https://doi.org/10.1016/j.aej.2019.10.003.
[48] S. Di Bartolo, R. Salvini, Multitemporal terrestrial laser scanning for marble extraction assessment in an underground quarry of the apuan alps (Italy), Sensors 19 (3) (2019) 450, https://doi.org/10.3390/s19030450.
[49] P. Ziolkowski, J. Szulwic, M. Miskiewicz, Deformation analysis of a composite bridge during proof loading using point cloud processing, Sensors 18 (12) (2018) 4332, https://doi.org/10.3390/s18124332.
[50] P.B. Boucher, I. Paynter, D.A. Orwig, I. Valencius, C. Schaaf, Sampling forests with terrestrial laser scanning, Ann. Bot. (2021), https://doi.org/10.1093/aob/mcab073 mcab073.
[51] T.P. Pitkänen, T. Piri, A. Lehtonen, M. Peltoniemi, Detecting structural changes induced by Heterobasidion root rot on Scots pines using terrestrial laser scanning, For. Ecol. Manag. 492 (2021) 119239, https://doi.org/10.1016/j.foreco.2021.119239.
[52] J.R. Rosell-Polo, E. Gregorio, J. Gené, J. Llorens, X. Torrent, J. Arnó, A. Escolà, Kinect v2 sensor-based mobile terrestrial laser scanner for agricultural outdoor applications, IEEE ASME Trans. Mechatron. 22 (6) (2017) 2420–2427, https://doi.org/10.1109/TMECH.2017.2663436.
[53] A.F. Colaço, R.G. Trevisan, J.P. Molin, J.R. Rosell-Polo, A. Escolà, A method to obtain orange crop geometry information using a mobile terrestrial laser scanner and 3D modeling, Rem. Sens. 9 (8) (2017) 763, https://doi.org/10.3390/rs9080763.
[54] J. Gené-Mola, E. Gregorio, F. Auat, J. Guevara, R. Sanz-Cortiella, A. Escolà, J. Llorens, J.P. Morros, J. Ruiz-Hidalgo, V. Vilaplana, J.R. Rosell-Polo, Fruit detection in an apple orchard using a mobile terrestrial laser, Biosyst. Eng. 187 (2019) 171–184, https://doi.org/10.1016/j.biosystemseng.2019.08.017.
[55] F. Auat Cheein, J. Guivant, R. Sanz, A. Escolà, F. Yandún, M. Torres-Torriti, J. R. Rosell-Polo, Real-time approaches for characterization of fully and partially scanned canopies in groves, Comput. Electron. Agric. 118 (2015) 361–371, https://doi.org/10.1016/j.compag.2015.09.017.
[56] G. Pérez, *Façanes vegetades. Estudi del seu potential com a sistema passiu d'estalvi d'energia, en clima mediterrani continental"*. PhD thesis, Universitat Politècnica de Catalunya, 2010. https://www.tdx.cat/handle/10803/6144#page=1.
[57] M. Manso, J. Castro-Gomes, Green wall systems: a review of their characteristics, Renew. Sustain. Energy Rev. 41 (2015) 863–871, https://doi.org/10.1016/j.rser.2014.07.203.
[58] A. de Gracia, L. Navarro, J. Coma, S. Serrano, J. Romaní, G. Pérez, L.F. Cabeza, Experimental set-up for testing active and passive systems for energy savings in buildings – lessons learnt, Renew. Sustain. Energy Rev. 82 (1) (2018) 1014–1026, https://doi.org/10.1016/j.rser.2017.09.109.
[59] F. Bosché, A. Mahmound, Y. Turkan, C.T. Haas, R. Haas, The value of integrating Scan-to-BIM and Scan-vs-BIM techniques for construction monitoring using laser scanning and BIM: the case of cylindrical MEP components, Autom. ConStruct. 49 (2015) 201–2013, https://doi.org/10.1016/j.autcon.2014.05.014.
[60] A. Fernández-Sarría, L. Martínez, B. Velázquez-Martí, M. Sajdak, J. Estornell, J. A. Recio, Different methodologies for calculating crown volumes of *Platanus hispanica* trees using terrestrial laser scanner and a comparison with classical dendrometric measurements, Comput. Electron. Agric. 90 (2013) 176–185, https://doi.org/10.1016/j.compag.2012.09.017.
[61] J. Guevara, F.A. Auat Cheein, J. Gené-Mola, J.R. Rosell-Polo, E. Gregorio, Analyzing and overcoming the effects of GNSS error on LiDAR based orchard parameters estimation, Comput. Electron. Agric. 170 (2020) 105255, https://doi.org/10.1016/j.compag.2020.105255.
[62] A. Miranda-Fuentes, J. Llorens, J. Gamarra-Diezma, J. Gil-Ribes, E. Gil, Towards an optimized method of olive tree crown volume measurement, Sensors 15 (2015) 3671–3687, https://doi.org/10.3390/s150203671.